Forward-Looking Ultrasound Imaging Transducer : II. Fabrication and Experimental Results

Chankil Lee*

ABSTRACT

The experimental testing results of the large-scale version of a forward-looking ultrasound imaging catheter (FLUIC) are presented, along with the fabrication techniques used, experimental methods, and comparisons of the measured and simulated results. The transducer model is verified by measuring the electrical impedance of the transducer. The pulse width, beamwidth, and the dynamic range for both transmit and pulse-echo response of the fabricated FLUIC are also analyzed. The experimental results conformed its forward-looking imaging capability and the sources of discrepancies between the simulated and experimental beam profiles are addressed.

Ⅰ. Introduction

In a previous companion paper [1], the analysis and design of a forward-looking ultrasound imaging catheter (FLUIC) were presented. To predict the fied characteristics of the FLUIC, a computationally efficient model was developed and the accuracy of the model was verified by simulation and experiment through a simple plane reflector. However the measured characteristics of a FLUIC were not given. The purpose of this paper is to provide the fabrication techniques used for a FLUIC, experimental methods, and comparisons of the measured and simulated results.

Ⅱ. Fabrication

The transducer and scanning section of the large-scale FLUIC were fabricated. The scanning section was devised to provide both rotational and translational scanning. It consists of a rotator(Newport, RSA-1), translator (Newport, 461-X), and rotating shaft, as shown in Fig. 1 (a).

The rotator holds the rotating shaft to provide the rotational scanning. The rotator was mounted on the top of the translator to provide additional translational scanning. The assembled scanning section was mounted on the supporter which was attached to the side wall of the water tank(Medisonics (UK) Ltd., $25cm \times 25cm \times 60cm$).

The transducer section consisted of a conical mirror and piezoelectric ceramic disk, as shown in Fig.1(b). The mirror, mounted at the side wall of the water tank, was made of polished stainless steel so that the reflected wave could considered as a specular reflection. The dimensions of the mirror are described in [1].

The piezoelectric ceramic disk (Valpey-Fisher, overtone polished Chromium/Gold coax electroding) was measured by a micrometer to have a radius and thickness of $5mm$ and $1.05mm$, respectively. The lowest antiresonance frequency was approximately by 2.0MHz. Lead/tin solder was used to connect the piezoelectric ceramic to the coaxial connector (Pasternack PE4014) via a $20cm$ long, 50Ω miniature coaxial cable (Belden RG-174U). The sensitive area of a piezoelectric ceramic was estimated by measuring the free-space capacitance. The measured capacitance, $C_T = 947pF$, indicated that the effective radius was $a = 4.59mm$, which was less than the plysical radius. The coaxial cable through a groove cut along the length of the rotating shaft.

For back-load matching, the backing material was made of epoxy/polyamide resin (Locite Corp.) and tungsten powder filter (Teledyne Wah Chang). The tungsten powder was mixed with the epoxy and poured into a sample holder. The composite had a total volume fraction of about 30% and a filler particle size range of $3 \sim 5\mu m$. The composite was hand polished using polishing paper to form flat surface. To determine the acoustic impedance of the backing material, its density was calculated by measuring its volume and weight. Next, the sound velocity in the composite was measured by the transmission method using two plane transducers (transmitter : Panametrics A301S 0.5MHz, receiver : Megasonics 10MHz) coupled it

*Department of Electronics, Hanyang University
Manuscript Received May 9, 1996.

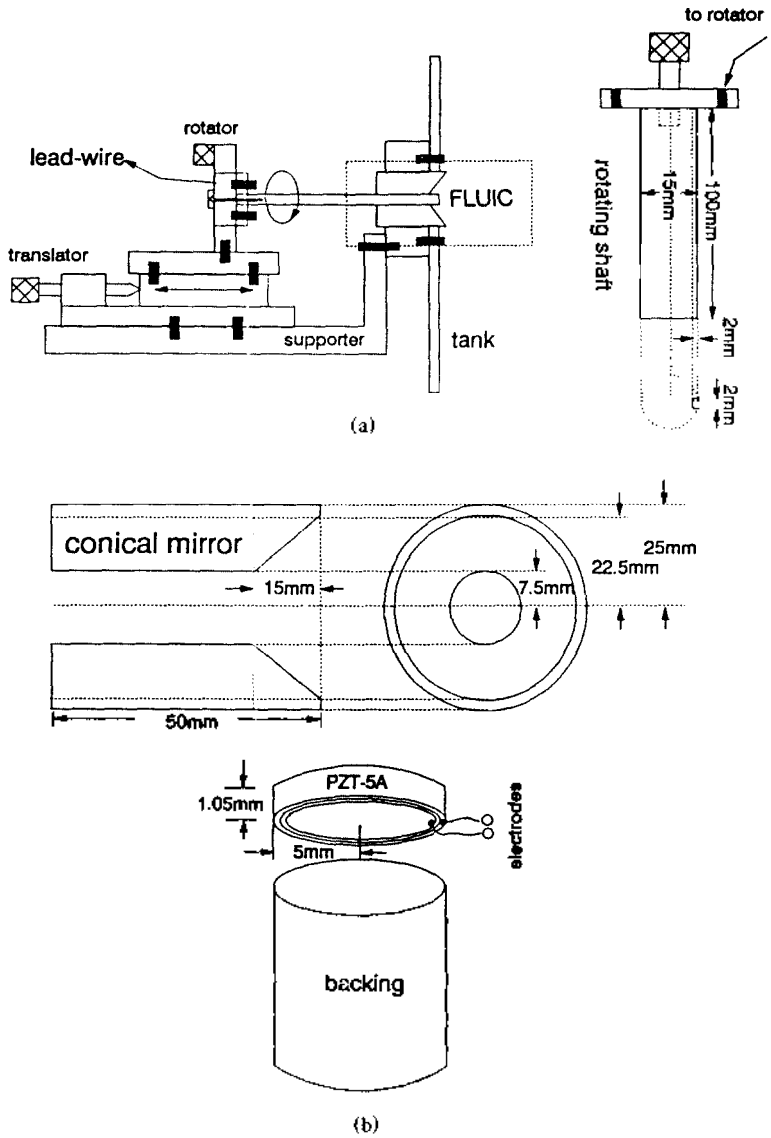

Fig 1. Diagram of the fabricated large-scale version of the FLUIC : (a) scanning and (b) transducer section.

with ultrasonic gel (Parker Lab.). The measured density density and velocity of the backing material were approximately 5.2kg/m^3 and 1375m/s, respectively, resulting in the acoustic impedance of 7.15kg/m^2-s. The backing was bonded to the piezoelectric ceramic and to the rogtating shaft with thin layers of the same epoxy/tungsten mixture. The acoustic impedance matching in a front load and electrical tuning circulit was not considered in this fabrication.

Ⅲ. Experimental Methods

To test the large-scale FLUIC, a general-purpose ultrasonic data acquisition system, as shown in Fig.2, was employed. It consisted of the rotational and translational stages of the FLUIC, a broadband ultrasonic analyzer (Panametrics 5052UA) for a pulse excitation, a function generator (Wavetek 143) for CW excitation, a 250 Msamples /sec digital oscilloscope (Tektronix 2432), and a 3-D positioning mechanism (Velmex Inc., Alpha Products SC-149) with a maximum resolution of 25.4μm for the hydrophone probe or test phantom. A mirocomputer (IBM PC/XT) controlled the procedure required for data acquisition and positioning via an IEEE 488 (Metrabyte IE488) and A-bus interface (Alpha Products) cards, respectively. All measurements were made in a water tank. The water was partially degassed and brought to room temperature by allowing it to sit for 72 hours or longer.

The ultrasonic data acquisition system operated in two

modes. To characterize the field of the large-scale FLUIC, a needle hybrophone (NTR System Inc., Model TNU100A) was scanned through the field to measure the acoustic pressure as shown in Fig.2 (a). The hydrophone consists of a 1-*mm* diameter piezoelectric ceramic element mounted in a submersible probe.

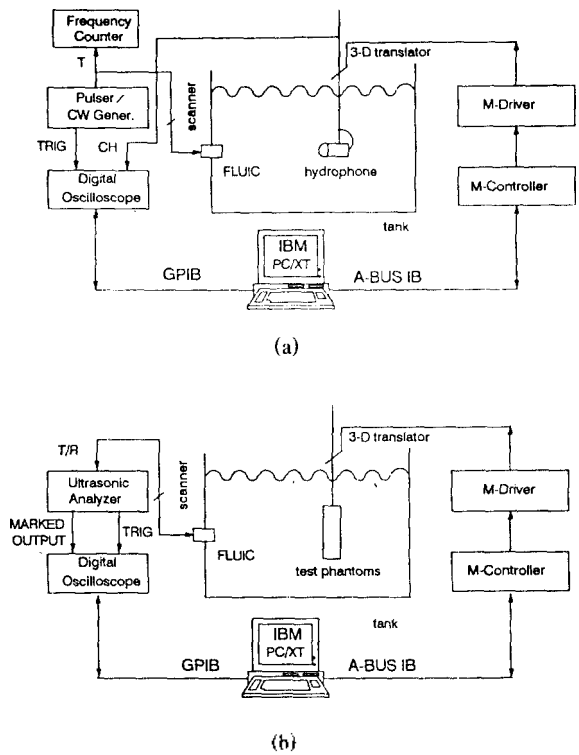

Fig 2. Experimental setup for ultrasonic data acquisition. (a) Transmission mode. (b) Pulse-echo mode.

The function generator drove the FLUIC with a CW signal. The output of the generator was monitored by a frequency counter (Hewlett-Packard 5314A). The output of the hydrophone was measured by the digital oscilloscope and was stored on the hard disk of the microcomputer.

To examine the pulse-echo response of the large-scale FLUIC, simple test phantoms, consisting of stainless steel balls, were devised. These allowed the resolutions in the transverse and elevation dimensions to be evaluated. The system shown in Fig.2 (b) was used to collect the pulse-echo data. The ultrasonic analyzer drove the FLUIC with short pulses and received the backscattered echo signals from the balls. These signals were amplified by the analyzer and sampled at a rate of 250 Msamples/sec. The measured rms values were stored on the hard disk of the microcomputer. C-scan images were constructed to evaluate the imaging capabilities of the FLUIC using three steel balls.

Due to resource limitations, manually operated optical rotational and translational stages were employed to mechanically scan the FLUIC. Ultimately, this scanning will be accomplished by stepped motors under computer control to reduce the data acquisition time.

Ⅳ. Experimental Results

A good medical imaging transducer has a high sensitivity, generates short acoustic pulses to achieve a high axial resolution and has narrow beamwidth characteristics for high lateral resolution. The sensitivity and bandwidth of the transducer are dictated by the characteristics of the piezoelectric transducer material used, as well as by the transducer backing and the electrical and acoustical impedance matching devices. Therefore, the transducer model as discussed in [1] was verified by measuring the electrical impedance of the transducer. The pulse width, beamwidth, and the dynamic range for both transmit and pulse-echo response of the fabricated FLUIC were also analyzed.

For the value of the SPICE (Simulation Program with Intetrated Circuit Emphasis) simulation of the FLUIC's transducer, the following parameters were used:

$$A = \pi a^2 = 0.63 \times 10^{-6}\ m^2\ Z_o = \rho v_{33}^D A = 2.14 \times 10^3\ N/(m/s)$$
$$\tau = l / v_{33}^D = 0.241\ \mu\text{sec}$$
$$C_o = \varepsilon^S\ A/l = 445 pF\ h C_o = e_{33} C_o / \varepsilon^S = 0.957\ N/V$$

1. Electrical Impedance

The electrical impedance of the PZT-5A disk employed in the FLUIC was measured by a vector impedance meter (Hewlett-Packard 4193A). The leads were attached to the impedance meter by means of a supplied connector. The data acquisition was computer controlled via IEEE-488 interface card. A BASIC control program stepped through the desired frequencies at 2KHz increments and stored the data on the disk.

To verify the simulation model (based on the Redwood model, as discussed in [1]) the transducer was tested under a variety of mechanical load conditions; (a) air on each side, (b) loaded by water on each side, and (c) loaded by water and the composite backing. The theoretical value of the impedance was calculated using the constants given in Table 1 [1], for comparative purposes. For the case of the unloaded case, $f_a = 1.95$MHz and $f_r = 2.13$ MHz, as shown in Fig.3. From these values, assuming a one dimensional thickness-mode vibration, the coupling

factors and velocity of the transducer can be estimated as $k_T = 0.438$ and $v_{33}^D = 4473\, m/s$, respectively, using equations derived in [1]. The thickness-mode assumption does not hold well for the unloaded transducer since the surface normally breaks up into anhramonic modes often associated with high overtones of lateral modes. These can be observed as relatively large spurious responses superimposed on the main thichness-mode response [2], as shown in Fig.3.

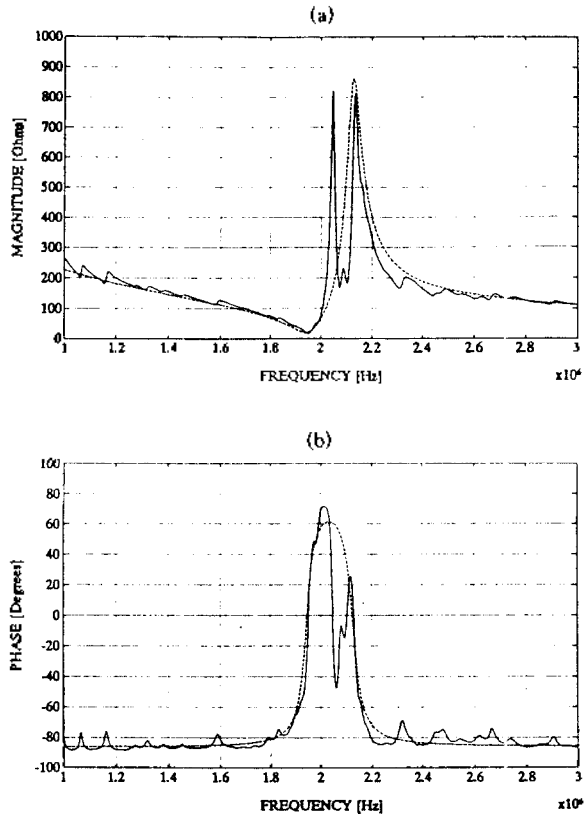

Fig 3. The electrical impedance of the unloaded FLUIC's transducer (solid : measured, dashed : simulated). (a) Magnitude. (b) Phase.

However, the one-dimensional analysis applies surprisingly well to the loaded transducer where these anhamornic modes tend to suppressed. As expected, the magnitude of the impedance reaches a minimum near the resonance frequency and a maximum near its antiresonance frequency. As the degree of backing impedance matching is improved, the impedance profile becomes very broad and the shorter pulse can be generated, as shown in Figs.4 and 5.

The bandwidth of the fabricated transducer can be determianed by using the measured impedance profile. The calculated bandwidth (-3 dB) of the acoustic output power delivered by the transmitter with impedance 50Ω

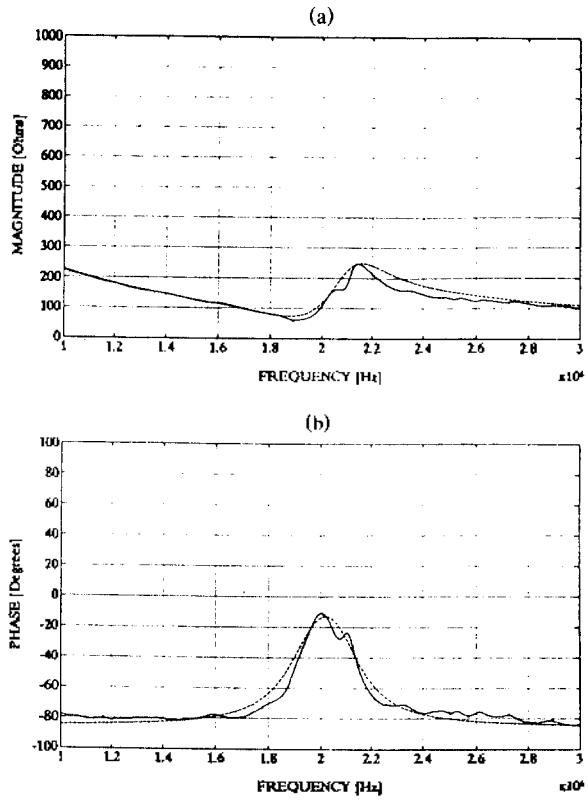

Fig 4. The electrical impedance of the FLUIC's transducer loaded by water (solid : measured, dashed : simulated). (a) Magnitude. (b) Phase.

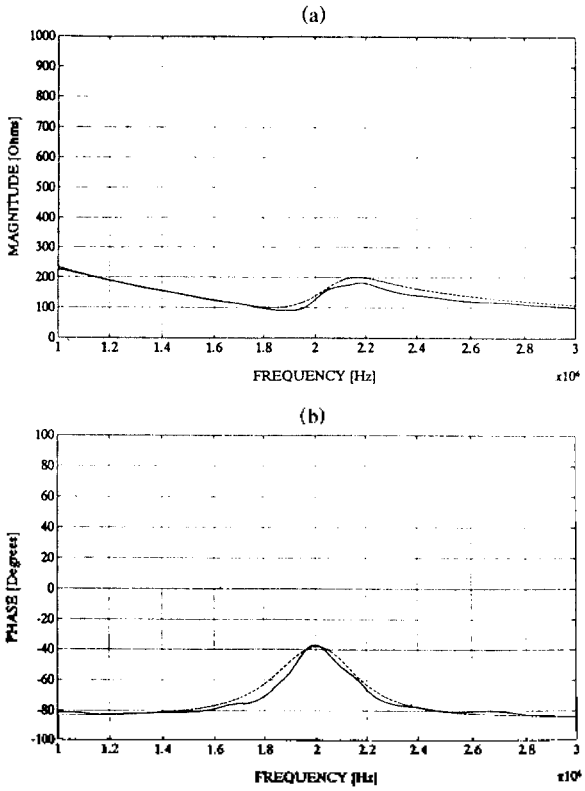

Fig 5. The electrical impedance of the FLUIC's transducer loaded with a front load of water and composite backing (solid : measured, dashed : simulated). (a) Magnitude. (b) Phase.

was about 0.4 MHz, as shown in Fig.6. The discontiuities at 1.25 MHz and 2.8 MHz in this figure were due to to software errors in collecting the data from the vector impedance meter.

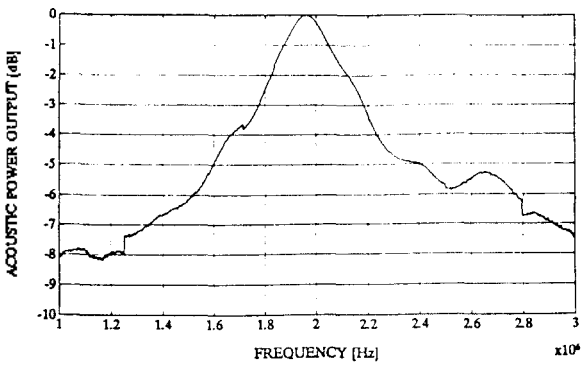

Fig 6. The acoustic output power of the FLUIC's transducer for the transmitter impedance 50Ω.

2. Axial Resolution

A monofilm hydrophone (NTR Systems Inc., Model TMU010A) was employed to detect the transducer electromechanical response. The response of the hydrophone was flat between 1 and 12 MHz. The hydrophone was connected directly to the oscilloscope amplifier via a short length of coaxial cable, hence ensuring that electrical load effects did not distort the hydrophone response. To minimize the diffraction effects, the hydrophone was placed in close proximity to the front face of the transducer.

To simulate the electromechanical response of the large-scale FLUIC, the excitation signal(i.e. the output of the ultrasonic analyzer), as shown in Fig.7 (a), was stored by the digital oscilloscope and used as an input to the SPICE simulation. The simulation result, shown in Fig.7 (b), reproduces reasonably well the measured response. The discrepancies between the simulated and measured data in this figure were due primarily to three sources: the incomplete characterization of the pulser and transducer, cable effects (which were not included in the simulation), and finally the possibility of radial vibrations in the ceramic disk. In this comparison, the first part of the measured signal was removed due to its contamination by electrical coupling interference and reflections from the hydrophone surface. From this result, the -3 dB axial resolution of the fabricated transducer is about 1 μs, or 1.5mm. The axial resolution can be improved further by employing acoustic impedance matching and electrical tuning techniques.

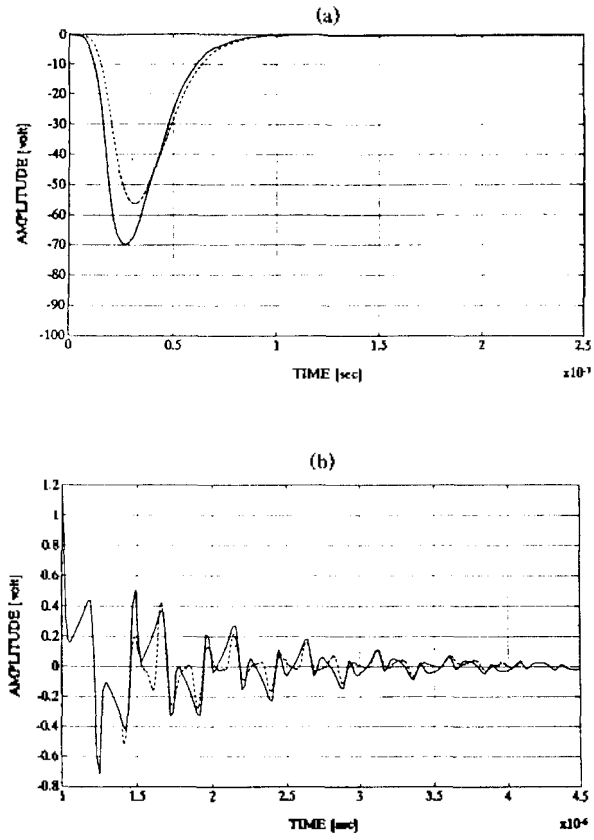

Fig 7. The electromechanical response of the FLUIC's transducer. (a) Excitation signal (solid: unloaded, dashed: loaded by transducer). (b) Simulated and measured transient response (solid: simulated, dashed: measured).

3. Lateral Resolution

Experimental measurements of the field pressure distributions of the large-scale FLUIC were made and compared with the corresponding simulation data. The experiment was performed by fixing the transducer element's position at the center of the mirror ($\phi = 0$) and scanning the hydrophone in the xy plane. Figure 8 shows the field patterns at z positions 30, 40, and 50 λ from the FLUIC.

Each beam pattern is normalized by the peak value at each z range and compared with the simulated data in [1]. The differences between the measured and simulated lateral resolutions are on the order of λ. The asymmetry in experiments mainly arises from misalignment of the hydrophone probe's translational axes. In addition, errors in positioning the probe in the z dimension affected the overall agreement between the measured and simulated data. The broadening of a field pattern in the measured data was a result of the spatial averaging effect of the finite aperture size of the hydrophone (1-mm diameter) $\lambda = 0.75mm$).

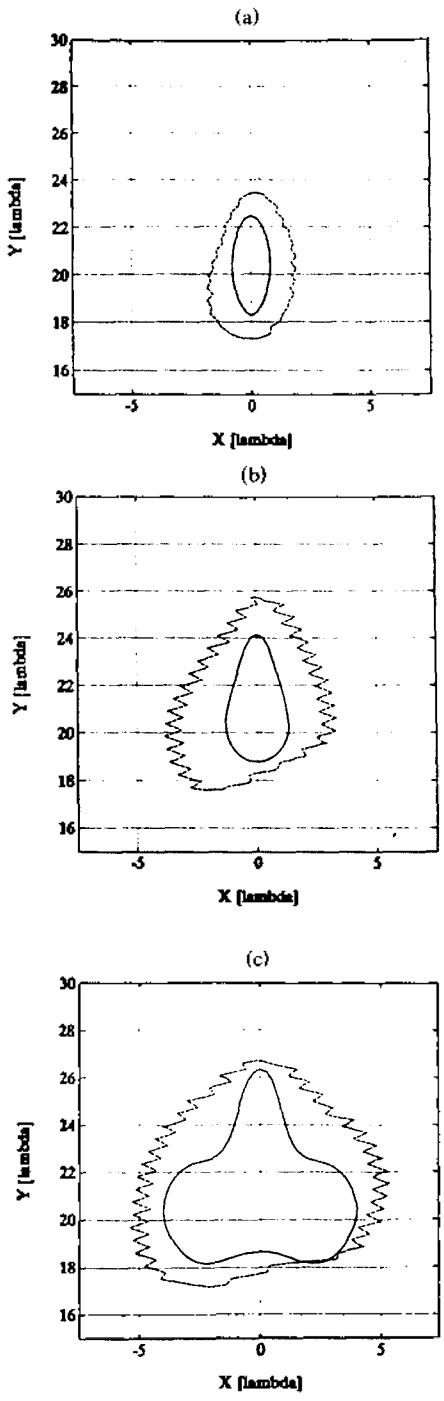

Fig 8. Contour plot (-3 dB) of the transmit characteristic at : (a) $z = 30\lambda$: (b) $z = 40\lambda$; and (c) $z = 50\lambda$ (solid : simulated CW, dashed : measured CW).

Several pulse-echo measurements using steel balls (diameter $= 0.7mm \approx \lambda$) were made. Although a general approach to predict the pulse-echo response was discussed [3], a rigorous prediction is difficult since the scattering characteristics of an object and the response of the transmit /receive electronics must be known. Figure 9 shows the typical transmitted pulse detected by the hydrophone and the echo signal from a steel ball at the same position. Although the steel ball was not a point scatterer (diameter $\ll \lambda$), the pulse-echo signal is still a convolutional form of the transmitted pulse, as discussed in [1].

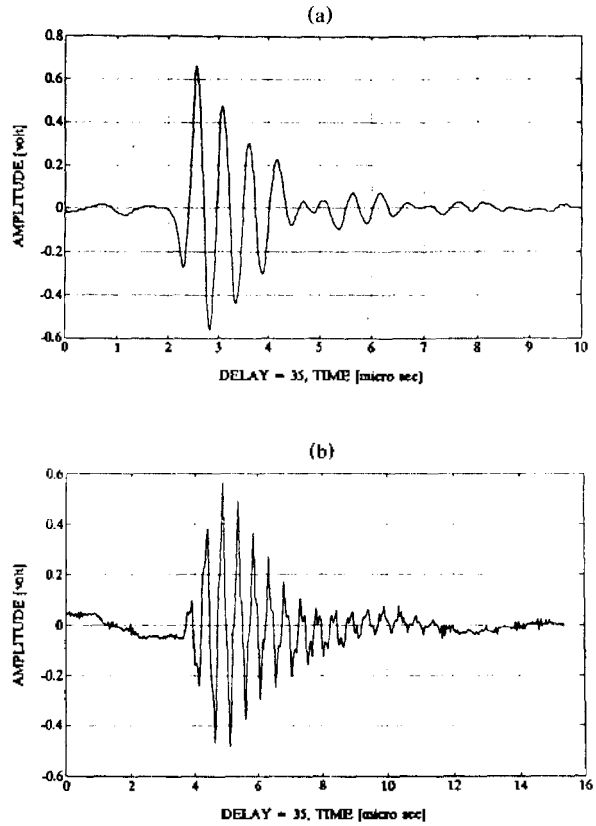

Fig 9. The typical pulse characteristics of a FLUIC at $z = 30\lambda$. (a) Transmitted pulse scanned by hydrophone. (b) Echo from a steel ball.

To compare the simulation and measured results for pulse-echo response characteristics, the square of the transmit transfer function was employed. As discussed in [1], CW simulation can be used to predict the approximate beamwidth of the pulse-echo response. Figure 10 shows a comparsion of the simulated CW two-way response and the measured pulse-echo response from the steel ball. The differences between the measured and simulated lateral resolutions are less than λ.

In addition to the problems similar to those associated with CW measurement, the broadening of the beam characteristics is also partly due to the finite of the scatterer. The characteristic frequency used in the simulation may be different from the actual mean frequency of the excitation spectrum. Thus, the approximate CW simulation using the different wavelength may also affect

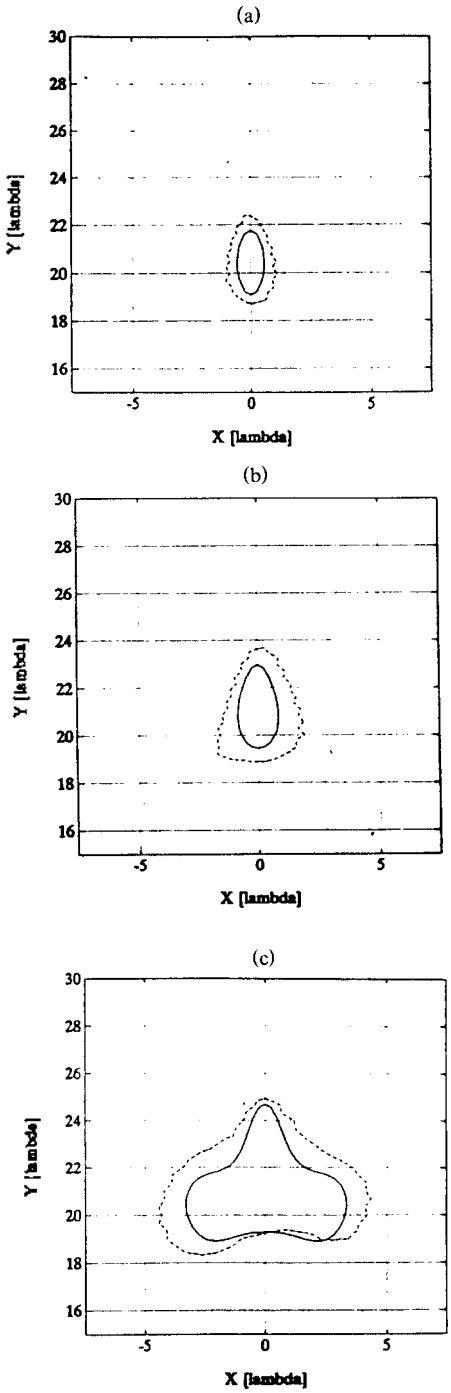

Fig 10. Contour plot (-3 dB) of the pulse-echo response at : (a) $z = 30\lambda$; (b) $z = 40\lambda$; and (c) $z = 50\lambda$ (solid : simulated CW, dashed : measured pulse-echo).

the beam profile.

Figure 11 shows the C-scan image of three steel balls separated in the x direction by $3mm$ and $5mm$, at $z = 30\lambda$. In the image formation, the rms values were calculated from the backscattered signal. The transverse resolution, defined by the -3 dB beamwidth, at $z = 30\lambda$ provides $2\pi(20\lambda)/\lambda \approx 125$ scan points, which is about 2.88° resolution. However, the image quality in the radial dimension would be relatively poor due to low elevation resolution. The ghost image between the two left steel balls comes from the finite lateral resolution of the transducer.

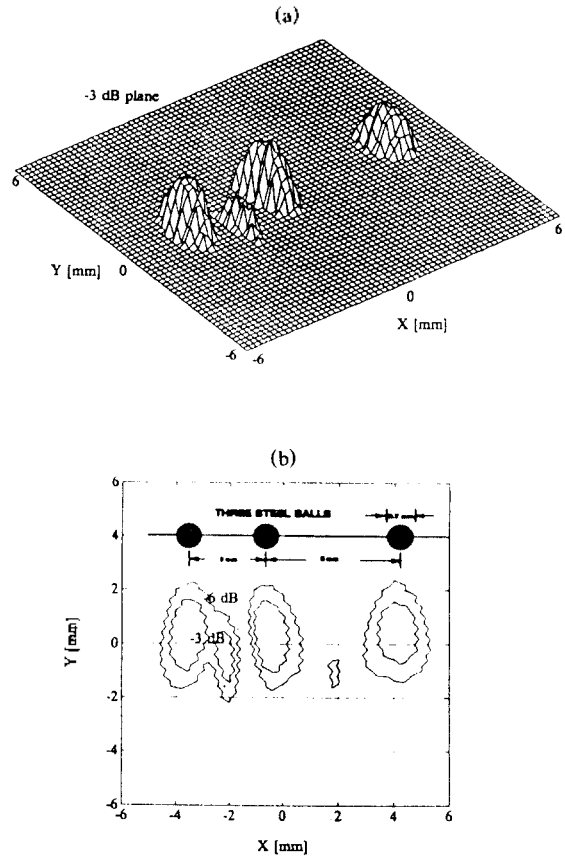

Fig 11. Image formation of a test object consisting of three steel balls separated at $z = 30\lambda$ by : (a) $3mm$; and (b) $5mm$.

4. Dynamic Range

Since the echo imaging system should only be sensitive to targets positioned along the direction of the main beam, the background noise will reduce the dynamic range available for unambiguous imaging. The reduction in dynamic range is a serious problem in diagnostic imaging where large variations in echo amplitudes from adjacent structures within the body are frequently encountered.

The dynamic range for the system can be defined in terms of the main lobe to peak side lobe ratio and expressed logarithmically as

$$DR = 20\log[(ML/SL)_T\,(ML/SL)_R]$$

where ML is the peak value of the main lobe, SL is the

peak value of the largest largest side lobe, and the subscripts T and R refer to the main lobe to side lobe ratios in the transmitting and receiving modes, respectively [4].

Figure 12 shows the lateral field patterns scanned by $-10mm < x < 10mm$ at($y = 1.5mm$, $z = 2.25mm$). The dynamic range at this field point was about 25 dB using the first side lobe level. The background level of the measured response was about 35 dB, which is determined mainly by the resolution of the digital oscilloscope. Although this dynamic range appears sufficiently large for imaging of the strong scattering targets, signal compression techniques used to image the weak-scattering targets can also enhance the contrast. The distributed targest within the body also lower the dynamic range as a result of reverberant artifacts, as shown in Fig.11.

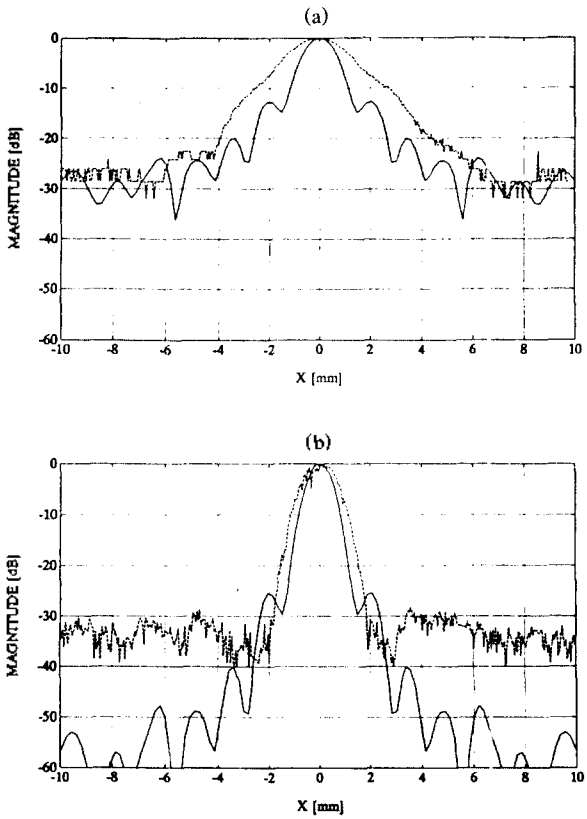

Fig 12. The lateral field patterns at ($y = 1.5mm$, $z = 2.25mm$) (solid : simulated, dashed : measured). (a) CW response. (b) Pulse-echo response.

V. Conclusions and Future Work

The initial experimental testing of a large-scale version of the FLUIC confirmed its forward-looking imaging capability. However, there were small differences between the simulated and experimental beam profiles. Additional research is needed to confirm that the source(s) of these discrepancies were due to : (1) misalignment of a motor translational axis ; (2) positioning errors of the probe with respect to the center of the FLUIC ; (3) and fabrication errors such as misalignment of the transducer element.

A motorized rotator and translator are needed to rapidly acquire the echo waveforms. Acoustical matching and an electrical tuning circuit should be added for future FLUIC designs to improve the axial resolution and dynamic range. To better evaluate the resolution and dynmic range of the FLUIC, more complex/realistic test phanotoms should be designed. Further work is needed to optimize the design of the mirror of the FLUIC. This would include include a complete investigation of alternative mirror configurations. In addition, nonvascular applications, both medical and NDE, should be considered to find other potential uses of the FLUIC. Ultimately, once a prototype has been designed and fabricated, vessel phantoms/animal studies will have to be conducted before a final determination can be made on whether to proceed with the development of a clinical prototype.

Further research is also needed to study the potential limitations in accurately machining a FLUIC in the 4~9 Fr range. The limitations in machining technology may determine the limits on the miniaturization of the FLUIC.

REFERENCES

1. C.K.Lee, "Forward-Looking Ultrasound Imaging Transducer : I.Analysis and Design," *J. Acoust. Ko.*, vol. 14, no. 2e, pp. 73-86, 1995.
2. D.A. Berlincourt, D.R. Curran, and H. Jaffe, Physical Acoustics, Vol. 1, *Academic Press*, 1964.
3. P.R. Stepanishen, "Pulsed transmit/receive response of ultrasonic piezoelectric transducers," *J. Acoust. Soc. Am.*, vol. 69, no. 6, pp. 1815-1827, 1981.
4. O.T.V. Ramm and S.W. Smith, "Beam steering with linear arrays," *IEEE Trans. Biom. Engr.*, vol. 30, no. 8, pp. 438-452, 1983.

▲Chankil Lee

Chankil Lee received the B.S. degree in electronic engineering from Hanyang University in 1981, and the M.S. degree from the Seoul National University in 1983 and the Ph.D. degree from Georgia Institute of Technology, Atlanta, Georgia, in 1992. From 1983 to 1985, he was involved in development of TDX-1 ESS at ETRI. During 1986-1992, he worked on the radio signal processing and the diffraction problems of acoustic radiators. In 1992, he joined the Radio Technology Department at ETRI, where he worked on CDMA mobile radio systems. Since 1995, he has been an Assistant Professor at the Department of Electronic Engineering, Hanyang University, Ansan. His research interests include wave propagation and diffraction theory, multipath fading channel characterization, and wireless communication link design.